

Ignition Processes in Hydrogen-Oxygen Mixtures

U. MAAS and J. WARNATZ

*Physikalisch-Chemisches Institut der Universität Heidelberg, Im Neuenheimer Feld 253,
6900 Heidelberg, West Germany*

Ignition processes in the hydrogen-oxygen system were simulated by solving the corresponding conservation equations (i.e., conservation of mass, energy, momentum, and species mass) for one-dimensional geometries using a detailed reaction mechanism and a multispecies transport model. An additional source term in the energy conservation allowed the treatment of induced ignition, and a realistic model for the destruction of reactive species at the vessel surface was used to treat auto-ignitions in static reactors. Spatial discretization using finite differences and an adaptive grid point system led to a differential-algebraic equation system, which was solved numerically by extrapolation or by backward differencing codes. Comparisons with experimental works show that one common reaction mechanism is able to simulate shock-tube-induced ignitions (modeled by treating the reaction system as a homogeneous mixture heated up by the shock wave) as well as the three explosion limits of the hydrogen-oxygen system. Minimum ignition energies are calculated for various mixture compositions, pressures, radii of the external energy source, and ignition times, and it is shown that for long ignition times the "uniform pressure assumption" is a quite good approximation for computing minimum ignition energies.

INTRODUCTION

The hydrogen-oxygen system is an attractive object of study because its detailed reaction mechanism is well understood (in contrast, for example, to hydrocarbon oxidation), because it is the simplest realistic combustion system, and because of its potential role as a fuel.

Knowledge of the elementary reactions in the H_2-O_2 system (discussed in a series of reviews (for example, [1-3]), has been used successfully to solve zero-dimensional problems such as autoignition chemistry [4], and stationary one-dimensional problems such as flame propagation (for example [3, 5-12]) and flame stabilization [13]. As the simulation of time-dependent one-dimensional problems such as ignition requires much greater computational effort, only a few studies on ignition in the H_2-O_2 system are available in the literature. Oran et al. [14] studied minimum ignition energies in $H_2-O_2-N_2$ mixtures, showing an increase of ignition energies for decreasing ignition sources (in contrast to the results pre-

sented below). Wiriyawit and Dabora [15] considered ignition in H_2 -air mixtures with an unrealistic diameter $r = 0.5$ mm to avoid regrid procedures. Lutz et al. [16] studied the interaction of pressure waves with the flame front in H_2 -air mixtures with very large energy deposition. Operator splitting techniques are used in all of these studies.

However, the development of codes for integrating differential-algebraic equation systems now allows the globally implicit solution of time-dependent one-dimensional problems with detailed homogeneous and heterogeneous chemistry. Together with adaptive gridding, the technique leads to a reliable treatment of auto-ignition, as well as induced ignition.

CALCULATION METHOD

Auto-Ignition and Induction Times

Simulations of shock-tube measurements of induction times can be simplified because the mixture in the reaction zone may be regarded as nearly

homogeneous. This allows zero-dimensional modeling, and the conservation equations reduce to the differential-algebraic equation system:

conservation of mass

$$\rho v = \text{constant}; \quad (1)$$

conservation of energy

$$\frac{\partial T}{\partial t} - \frac{1}{\rho c_p} \frac{\partial p}{\partial t} + \frac{1}{\rho c_p} \sum_{i=1}^{n_s} \dot{\omega}_i h_i M_i = 0; \quad (2)$$

species mass conservation

$$\frac{\partial w_i}{\partial t} - \frac{\dot{\omega}_i M_i}{\rho} = 0, \quad (3)$$

where P = pressure, T = temperature, n_s = number of species, w_i = mass fraction of species i , M_i = molar mass of species i , $\dot{\omega}_i$ = molar scale rate of formation of species i , h_i = specific enthalpy of species i , ρ = density, v = volume of the mixture, and c_p = constant pressure specific heat capacity of the mixture.

These equations represent a differential-algebraic system containing one algebraic (Eq. 1) and $n_s + 1$ ordinary differential equations (Eqs. 2 and 3). The dependent variables are T , P , and w_k if the reaction volume is given, and T , v , and w_k if the pressure is given. The equation system can be solved numerically using the backward differentiation formula code DASSL [20] or the extrapolation code LIMEX [21]. Cpu times are less than 1 s on a CRAY-1 computer.

Induced Ignition and Minimum Ignition Energies

The ignition process is simulated mathematically by solving the corresponding system of conservation equations, which may be written as:

continuity

$$\frac{\partial \rho}{\partial t} + \text{div } \rho v = 0, \quad (4)$$

species mass

$$\rho \frac{\partial w_i}{\partial t} + \rho v \text{ grad } w_i + \text{div } j_i = \dot{\omega}_i M_i, \quad (5)$$

momentum

$$\frac{\partial \rho v}{\partial t} + \text{grad } P + \text{div } \bar{\Pi} + \text{div } (\rho v \circ v) = 0, \quad (6)$$

energy

$$\frac{\partial \rho h}{\partial t} - \frac{\partial P}{\partial t} + \text{div } (\rho v h) - v \text{ grad } p + \text{div } j_q + \bar{\Pi} : \text{grad } v = \dot{q}, \quad (7)$$

where h = specific enthalpy, ρ = density, \vec{v} = velocity, \vec{j}_q = heat flux, j_i = diffusion flux of species i , $\bar{\Pi}$ = stretch tensor, \dot{q} = source term for deposition of energy, and t = time.

The simulations are simplified by restricting them to one-dimensional geometries (infinite cube, infinite cylinder, or sphere) and using the ideal gas law. The convective terms of the conservation equations can be eliminated by a transformation into Lagrangian coordinates. The equation system then reads:

$$\frac{\partial r}{\partial \psi} - \frac{1}{\rho r^\alpha} = 0, \quad (8)$$

$$\frac{\partial \rho}{\partial t} + \rho^2 \frac{\partial}{\partial \psi} (v r^\alpha) = 0, \quad (9)$$

$$\frac{\partial v}{\partial t} + r^\alpha \frac{\partial p}{\partial \psi} - \frac{4}{3} r^\alpha \frac{\partial}{\partial \psi} \left(\rho \mu \frac{\partial}{\partial \psi} (v r^\alpha) \right) + 2\alpha r^\alpha \frac{v}{r} \frac{\partial \mu}{\partial \psi} = 0 \quad (10)$$

$$\frac{\partial T}{\partial t} - \frac{1}{\rho c_p} \frac{\partial P}{\partial t} - \frac{1}{c_p} \frac{\partial}{\partial \psi} \left(\rho r^{2\alpha} \lambda \frac{\partial T}{\partial \psi} \right)$$

$$+ \frac{r^\alpha}{c_p} \sum_{i=1}^{n_s} \rho w_i V_i c_{pi} \frac{\partial T}{\partial \psi} + \frac{1}{\rho c_p} \sum_{i=1}^{n_s} \dot{\omega}_i h_i M_i - \frac{4\rho\mu}{3c_p} \left(\frac{\partial v r^\alpha}{\partial \psi} \right)^2 + \frac{2\alpha\mu}{c_p} \frac{\partial}{\partial \psi} (v^2 r^{\alpha-1}) = \frac{\dot{q}}{\rho c_p} \quad (11)$$

$$\frac{\partial w_i}{\partial t} + \frac{\partial}{\partial \psi} (\rho r^\alpha w_i V_i) - \frac{\dot{\omega}_i M_i}{\rho} = 0 \quad (12)$$

$$P - \frac{\rho RT}{M} = 0, \quad (13)$$

where
cylinder
numerical
specific
pressure
= specific
velocity
ity of
The
dependent
calculated
one a
volume
replaced

$$\frac{\partial P}{\partial \psi} =$$

The c
and th
fulfill
ordina
system

$$\frac{\partial r}{\partial \psi} =$$

$$\frac{\partial P}{\partial \psi} =$$

$$\frac{\partial T}{\partial t} =$$

$$+$$

$$\frac{\partial w_i}{\partial t} +$$

with t
and w
The
has a

$$\dot{q} = \frac{D_s}{\tau_s}$$

$$\dot{q} = 0$$

where
= so

where $\alpha = 0$ for infinite cube, $\alpha = 1$ for infinite cylinder, $\alpha = 2$ for sphere, $r =$ radius, $n_s =$ number of species, $c_{pi} =$ constant pressure specific heat capacity of species i , $c_p =$ constant pressure specific heat capacity of the mixture. $h_i =$ specific enthalpy of species i , $V_i =$ diffusion velocity of species i , and $\lambda =$ thermal conductivity of the mixture.

The independent variables are t and ψ ; the dependent variables are r , T , P , w_i , v , and ρ . The calculations can be simplified to a great extent if one assumes uniform pressure in the reaction volume. The momentum equation (10) then is replaced by the equation

$$\frac{\partial P}{\partial \psi} = 0. \quad (14)$$

The density ρ is substituted using equation (13), and the continuity equation (which is automatically fulfilled after transformation into Lagrangian coordinates) is no longer needed. The equation system simplifies to [17, 18]

$$\frac{\partial r}{\partial \psi} - \frac{1}{\rho r^\alpha} = 0 \quad (8)$$

$$\frac{\partial P}{\partial \psi} = 0 \quad (14)$$

$$\begin{aligned} \frac{\partial T}{\partial t} - \frac{1}{\rho c_p} \frac{\partial P}{\partial t} - \frac{1}{c_p} \frac{\partial}{\partial \psi} \left(\rho r^{2\alpha} \lambda \frac{\partial T}{\partial \psi} \right) \\ + \frac{r^\alpha}{c_p} \sum_{i=1}^{n_s} \rho w_i V_i c_{pi} \frac{\partial T}{\partial \psi} + \frac{1}{\rho c_p} \sum_{i=1}^{n_s} \dot{\omega}_i h_i M_i = \frac{\dot{q}}{\rho c_p} \end{aligned} \quad (15)$$

$$\frac{\partial w_i}{\partial t} + \frac{\partial}{\partial \psi} (\rho r^\alpha w_i V_i) - \frac{\dot{\omega}_i M_i}{\rho} = 0, \quad (13)$$

with t and ψ as independent variables, and r , T , P , and w_i as dependent variables.

The term for the artificial energy source, which has a nearly rectangular shape, is given by

$$\dot{q} = \frac{D_s}{\tau_s} \exp \left\{ - \left(\frac{r}{r_s} \right)^8 \right\} \text{ for } 0 < t \leq \tau_s \quad (11)$$

$$\dot{q} = 0 \text{ for } t > \tau_s \quad (12)$$

where r_s denotes the radius of the energy source, $\tau_s =$ source time, and $D_s =$ density of source

energy. This particular spatial shape for the artificial energy source is chosen to agree with measurements of the radial profile of the laser beam in corresponding experiments [18]. However, the code is not restricted to this particular choice.

For spherical and cylindrical geometries discussed in this paper, at the center of the reaction vessel ($\psi = 0$) symmetry conditions are used

$$r = 0$$

$$\frac{\partial T}{\partial \psi} = 0$$

$$\frac{\partial w_i}{\partial \psi} = 0.$$

In the case of nonuniform pressure, inner boundary conditions for the density and velocity are given by

$$\frac{\partial \rho}{\partial \psi} = 0$$

$$v = 0.$$

Because of the singularity at $\psi = 0$, resulting from the transformation into Lagrangian coordinates, these equations represent artificial boundary conditions.

Outer boundary conditions are simplified by assuming zero gradients of temperature and mass fractions at $\psi = \psi_0$:

$$\frac{\partial T}{\partial \psi} = 0$$

$$\frac{\partial w_k}{\partial \psi} = 0.$$

In the uniform pressure assumption there is one more boundary condition given by $r = R_0$. Otherwise, the remaining outer boundary conditions are given by

$$r = R_0$$

$$\frac{\partial P}{\partial \psi} = 0$$

$$v = 0$$

for a system at constant volume, and

$$P = P_0$$

$$\frac{\partial v r^\alpha}{\partial \psi} = 0$$

for a system with constant pressure at the outer boundary. R_0 denotes the radius of the reaction vessel, and P_0 the pressure at the outer boundary. An open boundary, allowing shocks to move out of the system and therefore simulating infinitely large reaction volumes, can be obtained by specifying

$$\frac{\partial P}{\partial \psi}$$

and

$$\frac{\partial v r^\alpha}{\partial \psi} = 0$$

at the outer boundary.

A system of coupled ordinary differential and algebraic equations is obtained by spatial discretization using finite differences and can be solved numerically. Adaptive gridding has to be used for simulations of ignition by artificial energy sources because of the large ratio of vessel diameter to flame front thickness and diameter of the artificial energy source. The method can be outlined as follows. A new grid point system is calculated after each time step. The grid point density is determined by equipartitioning the integral of a mesh function and inverse interpolation, with the mesh function F given by a weighted norm of gradients and curvature of the dependent variables f_m :

$$F(\psi) = \frac{\sum_{m=1}^M a_m \int_0^\psi \left| \frac{\partial f_m}{\partial \psi} \right| d\psi}{\int_0^{\psi_0} \left| \frac{\partial f_m}{\partial \psi} \right| d\psi} + b_m \frac{\int_0^\psi \left| \frac{\partial^2 f_m}{\partial \psi^2} \right| d\psi}{\int_0^{\psi_0} \left| \frac{\partial^2 f_m}{\partial \psi^2} \right| d\psi}, \quad (17)$$

where a_m and b_m are the weighting factors. In the present computations 60 grid points (40 of them for the case of uniform pressure) are distributed over the physical coordinate.

Stability is improved by inserting additional grid points if the ratio of two neighboring grid point intervals exceeds a certain value β ($\beta = 2$ in the present calculations)

$$1/\beta \leq \frac{\psi_{i+1} - \psi_i}{\psi_i - \psi_{i-1}} \leq \beta. \quad (18)$$

To ensure a sufficient number of grid points in the source volume, the radial distance in the first grid point interval must be less than a fifth of the source radius

$$r(\psi_2) \leq 0.2 r_s. \quad (19)$$

The number of grid points to be inserted or deleted in the old grid point system is then determined. If the old and new grid point system differ sufficiently, a new grid point system is generated by piecewise monotonic cubic hermite interpolation [19], and the integration is begun again. If there are only slight changes, the old grid point system is maintained and the integration is continued.

Simulations that do not assume uniform pressure are complicated by the problem of resolving the shock fronts. The thickness of shocks is about $1 \mu\text{m}$, and severe numerical instabilities result if the shock is not resolved. As we do not wish to resolve the shock front, we apply an artificial viscosity term ("numerical diffusion"), proposed by Richtmyer and Morton [22], which spreads the shocks over a certain number of grid points.

The system of ordinary differential and algebraic equations is again solved using the packages DASSL [20] or LIMEX [21]. As the integration has to be reinitiated after each adaptation of the grid point system, the one-step method LIMEX requires less computing time. The block tridiagonal structure allows an efficient numerical evaluation of the Jacobian, and the solution of the arising linear equation systems is performed by LU decomposition of the block tridiagonal iteration matrix.

Typical cpu times on a CRAY-1 computer are about 2 min for simulations of nonignition and

about 30 min for simulations of ignition in H₂-O₂ mixtures assuming uniform pressure, and more than 3 hours for simulations that do not assume uniform pressure.

P-T Ignition Limits

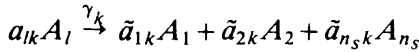
Modeling autoignition phenomena in closed vessels with one-dimensional geometries is done by solving the corresponding conservation equations (uniform pressure case) described above (Eqs. 8, 13-15). At the center of the reaction vessel ($\psi = 0$) symmetry boundary conditions are used:

$$r = 0$$

$$\frac{\partial T}{\partial \psi} = 0$$

$$\frac{\partial w_i}{\partial \psi} = 0. \quad (20)$$

In discussing autoignition phenomena in closed vessels, one has to take into account reactions that occur at the vessel surface, such as surface recombination of atoms or surface destruction of reactive molecules, as well as energy transfer to the vessel. If the reactions



occur with the probability γ_k when a particle of species A_l hits the surface, the formation rate of species i will be given by

$$\dot{\omega}_i^s = \sum_{k=1}^{n_s} \gamma_k Z_l M_i \{ \tilde{a}_{ik} - \delta_{li} a_{ik} \}, \quad (21)$$

where γ_k is the surface destruction efficiency, Z_l is the surface collision number of species l , a_{ik} is the stoichiometric coefficient of species i in reaction k , n_s is the number of surface reactions, and $\dot{\omega}_i^s$ is the mass scale rate of formation of species i per surface unit.

There is strong evidence that the overall mass flux j_i^s of species i vanishes at the surface. Therefore, the outer boundary condition for species mass conservation is given by

$$0 = j_i^s = \rho w_i V_i + \dot{\omega}_i^s. \quad (22)$$

The temperature at the outer boundary is assumed to be constant (maintained with a thermostat in experiments), and the system is considered to have a constant volume:

$$T(\psi_0) = T_0 \quad (23.1)$$

$$r(\psi_0) = R_0. \quad (23.2)$$

A coupled system of ordinary differential and algebraic equations is obtained by spatial discretization using finite differences with a fixed grid point system in ψ , and again solved numerically using the computer codes DASSL [20] or LIMEX [21]. These programs lead to the same results and require comparable computing times, less than 1 minute on a Cray-1.

Reaction Mechanism

Calculation was performed using a detailed mechanism for the gas phase reaction, consisting of 37 elementary reactions listed in Table 1 [35-37]. The rate coefficients were based on measurements available in the literature (see [35, 36] for further reference), and the rate coefficients of the reverse reactions were calculated using thermodynamic properties taken from the JANAF tables. No adjustments have been made to fit experimental results for explosion limits or ignition delay times, and the mechanism can also be used for modeling stationary flame propagation [38]. Measured data for surface reaction coefficients [23-25] differ very much and depend strongly on temperature, surface material, and the treatment of the surface before reaction (Table 2). In the calculations, rate coefficient values are varied within reasonable limits ($10^{-2} > \gamma > 10^{-4}$) to show the influence on the results.

RESULTS

Autoignition and Induction Times

Zero-dimensional simulations can be used to calculate ignition delay times of hydrogen-oxygen mixtures in shock tubes. As there exist extensive studies on this topic [4], we shall briefly present only a few results to validate the reaction mechanism used in this work to calculate ignition delay times.

TABLE I
Mechanism of the Hydrogen-Oxygen Reaction

	<i>A</i>	<i>β</i>	<i>E_a</i>
1. O ₂ + H → OH + O	2.00 × 10 ¹⁴	0.00	70.30
2. OH + O → O ₂ + H	1.46 × 10 ¹³	0.00	2.08
3. H ₂ + O → OH + H	5.06 × 10 ⁴	2.67	26.30
4. OH + H → H ₂ + O	2.24 × 10 ⁴	2.67	18.40
5. H ₂ + OH → H ₂ O + H	1.00 × 10 ⁸	1.60	13.80
6. H ₂ O + H → H ₂ + OH	4.45 × 10 ⁸	1.60	77.13
7. OH + OH → H ₂ O + O	1.50 × 10 ⁹	1.14	0.42
8. H ₂ O + O → OH + OH	1.51 × 10 ¹⁰	1.14	71.64
9. H + H + M → H ₂ + M	1.80 × 10 ¹⁸	-1.00	0.00
10. H ₂ + M → H + H + M	6.99 × 10 ¹⁸	-1.00	436.08
11. H + OH + M → H ₂ O + M	2.20 × 10 ²²	-2.00	0.00
12. H ₂ O + M → H + OH + M	3.80 × 10 ²³	-2.00	499.41
13. O + O + M → O ₂ + M	2.90 × 10 ¹⁷	-1.00	0.00
14. O ₂ + M → O + O + M	6.81 × 10 ¹⁸	-1.00	496.41
15. H + O ₂ + M → HO ₂ + M	2.30 × 10 ¹⁸	-0.80	0.00
16. HO ₂ + M → H + O ₂ + M	3.26 × 10 ¹⁸	-0.80	195.88
17. HO ₂ + H → OH + OH	1.50 × 10 ¹⁴	0.00	4.20
18. OH + OH → HO ₂ + H	1.33 × 10 ¹³	0.00	168.30
19. HO ₂ + H → H ₂ + O ₂	2.50 × 10 ¹³	0.00	2.90
20. H ₂ + O ₂ → HO ₂ + H	6.84 × 10 ¹³	0.00	243.10
21. HO ₂ + H → H ₂ O + O	3.00 × 10 ¹³	0.00	7.20
22. H ₂ O + O → HO ₂ + H	2.67 × 10 ¹³	0.00	242.52
23. HO ₂ + O → OH + O ₂	1.80 × 10 ¹³	0.00	-1.70
24. OH + O ₂ → HO ₂ + O	2.18 × 10 ¹³	0.00	230.61
25. HO ₂ + OH → H ₂ O + O ₂	6.00 × 10 ¹³	0.00	0.00
26. H ₂ O + O ₂ → HO ₂ + OH	7.31 × 10 ¹⁴	0.00	303.53
27. HO ₂ + HO ₂ → H ₂ O ₂ + O ₂	2.50 × 10 ¹¹	0.00	-5.20
28. OH + OH + M → H ₂ O ₂ + M	3.25 × 10 ²²	-2.00	0.00
29. H ₂ O ₂ + M → OH + OH + M	2.10 × 10 ²⁴	-2.00	206.80
30. H ₂ O ₂ + H → H ₂ + HO ₂	1.70 × 10 ¹²	0.00	15.70
31. H ₂ + HO ₂ → H ₂ O ₂ + H	1.15 × 10 ¹²	0.00	80.88
32. H ₂ O ₂ + H → H ₂ O + OH	1.00 × 10 ¹³	0.00	15.00
33. H ₂ O + OH → H ₂ O ₂ + H	2.67 × 10 ¹²	0.00	307.51
34. H ₂ O ₂ + O → OH + HO ₂	2.80 × 10 ¹³	0.00	26.80
35. OH + HO ₂ → H ₂ O ₂ + O	8.40 × 10 ¹²	0.00	84.09
36. H ₂ O ₂ + OH → H ₂ O + HO ₂	5.40 × 10 ¹²	0.00	4.20
37. H ₂ O + HO ₂ → H ₂ O ₂ + OH	1.63 × 10 ¹³	0.00	132.71

A has units of cm mole s; *E_a* has units of kJ mole⁻¹; $k = AT^\beta \exp(-E_A/RT)$.

Collision efficiencies in reactions with M: $f_{H_2} = 100$; $f_{O_2} = 0.35$; $f_{H_2O} = 6.50$; $f_{N_2} = 0.5$.

Figure 1 shows calculated ignition delay times compared with experimental results in shock tubes [26, 27] for hydrogen-oxygen-argon mixtures. Calculated induction times are in agreement with the experimental results. Sensitivity tests (Fig. 2) show the rate-limiting elementary reactions at 900 K, 1100 K, and 1500 K. At high and low temperatures the main rate-limiting process is the chain branching reaction



which dominates at high temperatures. At intermediate temperatures (1100 K) the chain branching reaction R1 competes with the chain terminating reactions R15 and R19:



The rates of other reactions exert only a minor influence on the ignition delay times.

TABLE 2

Surface Reactions in the Hydrogen-Oxygen Reaction

38.	$\text{HO}_2 \xrightarrow{w} \frac{1}{2} \text{H}_2\text{O} + \frac{3}{4} \text{O}_2$	γ_{38}
39.	$\text{O} \xrightarrow{w} \frac{1}{2} \text{O}_2$	γ_{39}
40.	$\text{H} \xrightarrow{w} \frac{1}{2} \text{H}_2$	γ_{40}
41.	$\text{OH} \xrightarrow{w} \frac{1}{2} \text{H}_2\text{O} + \frac{1}{4} \text{O}_2$	γ_{41}
42.	$\text{H}_2\text{O}_2 \xrightarrow{w} \text{H}_2\text{O} + \frac{1}{2} \text{O}_2$	γ_{42}

See text for surface destruction efficiencies γ_i .

Induced Ignition and Minimum Ignition Energies

As a comparison between experimental and computational results [18] shows, the mathematical model described above is able to calculate minimum ignition energies in ozone-oxygen mixtures. For hydrogen-oxygen mixtures, experimental results are not yet available and therefore only computational results are presented. An example of a simulation of an igniting mixture (not assuming uniform pressure) is shown in Figs. 3 and 4. For short ignition times (1–10 μs), the ignition process may be characterized as follows (Figs. 3 and 4): In the heating period the temperature and pressure rise quickly in the source volume, the time being too short for the pressure to distribute

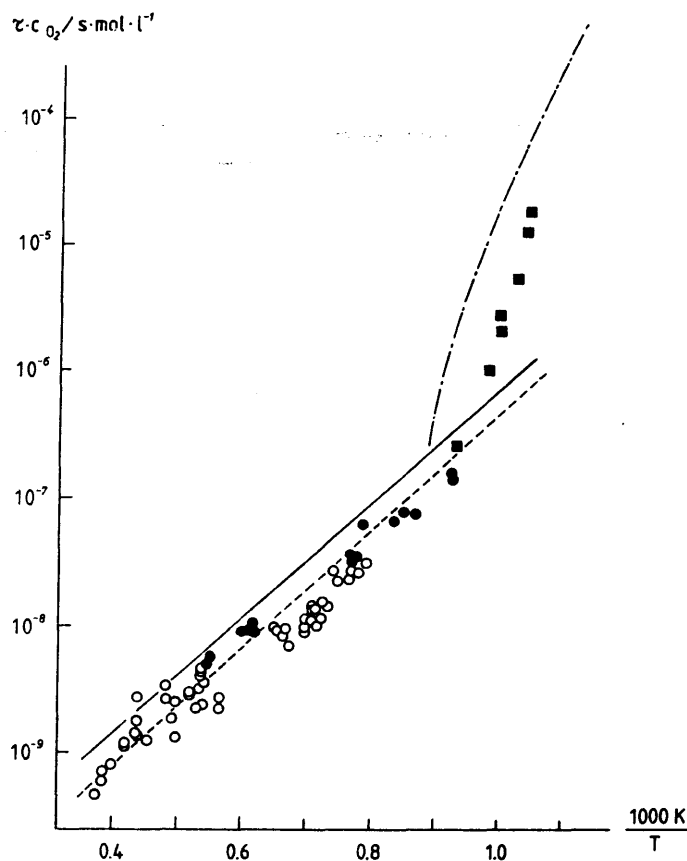


Fig. 1. Ignition delay times for hydrogen-oxygen-argon mixtures: (a) 8 % H_2 , 2% O_2 and 90% Ar, $P = 5$ atm: --- calculated, ■ experimental values [26]; criterion: maximum OH concentration (both in experiment and calculation); b) 4% H_2 , 2% O_2 and 94% Ar, $P = 1$ atm: -- calculated, ○ experimental values [27]; criterion: maximum change of OH concentration; c) 1% H_2 , 2% O_2 and 97% Ar, $P = 1$ atm: — calculated, • experimental values [27]; criterion: maximum change of OH concentration.

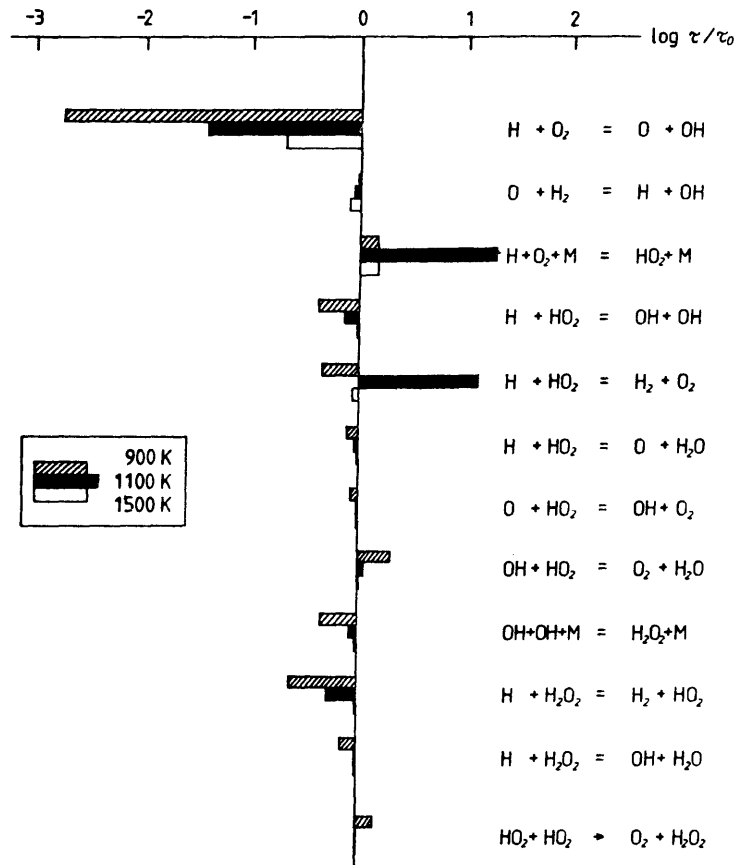


Fig. 2. Sensitivity test for ignition delay times in a hydrogen-oxygen-argon mixture (8% H₂, 2% O₂ and 90% Ar) at 1 bar; τ₀ refers to unchanged rate coefficients and τ refers to a tenfold increase of the rate coefficient of the reaction considered and its reverse reaction.

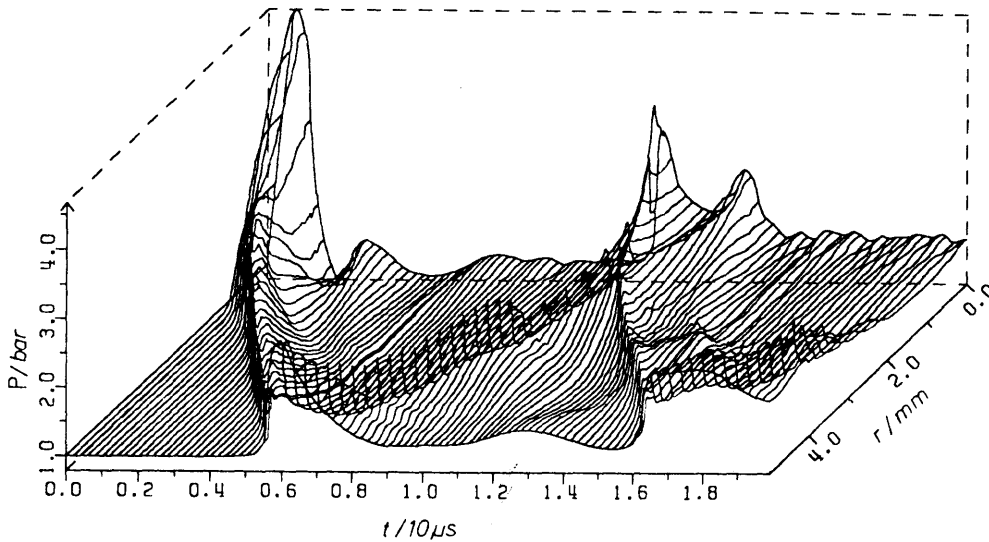


Fig. 3. Calculated pressure profiles in an igniting hydrogen-oxygen mixture (stoichiometric): cylindrical geometry, P = 1 bar, τ_s = 1 μs, r_s = 1 mm, E_s = 4J.

over the pressure profiles are the same at the outer boundary of the shock. The motion of the flame front is the "normal" movement, amplified due to the pressure rise. The pressure profiles allow the pressure equilibrium condition (via the law) to be inverted, capacity external, minimum ignition is ignition scale enough reaction

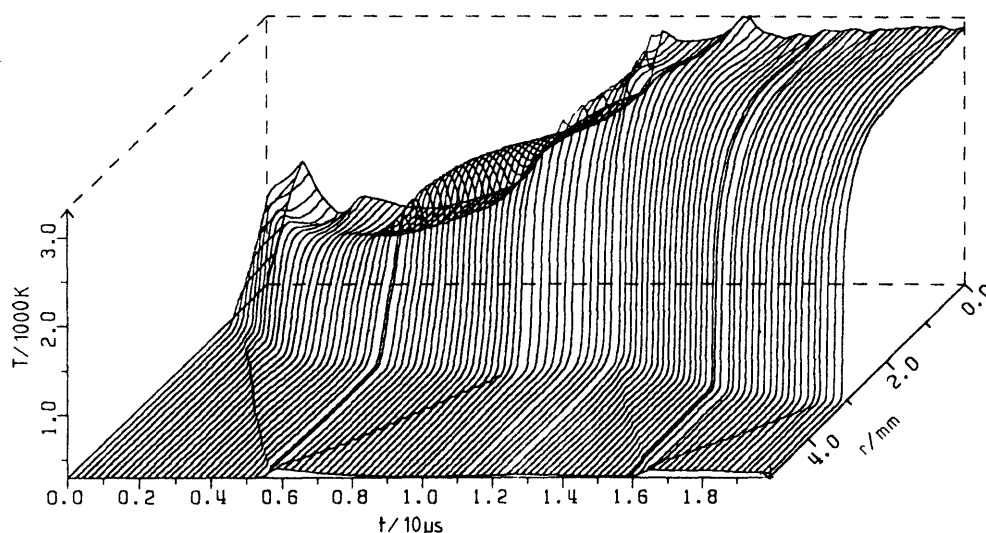


Fig. 4. Calculated temperature profiles in an igniting stoichiometric hydrogen-oxygen mixture: cylindrical geometry, $P = 1$ bar, $\tau_s = 1 \mu s$, $r_s = 1$ mm, $E_s = 4$ J.

over the whole volume of the mixture. A diverging pressure wave and a converging rarefaction wave are then formed. The rarefaction wave is reflected at the vessel center, forming a diverging wave, and the shock wave (moving in direction of the outer boundary) is reflected, forming a converging shock. The pressure waves perturb the propagation of the flame front, and the overall movement of the flame may be described as a superposition of the "normal" flame propagation and the oscillatory movements caused by the crossing shocks. The amplitude of the oscillations decreases with time due to the viscous forces.

The uniform pressure assumption does not allow the system to build up a region of high pressure in the source volume as the pressure is equilibrated instantaneously over the whole reaction volume. Because (according to the ideal gas law) the density is proportional to the pressure and inversely proportional to the temperature, the heat capacity per unit volume in the region of the external energy source and, therefore, also the minimum energies necessary to heat the mixture to its ignition temperature are smaller if the calculation is performed assuming uniform pressure. If ignition times are long in comparison to the time scale of the gas-dynamic processes, there is enough time for the pressure to equilibrate in the reaction system during the heating of the source

volume. The pressure is then uniform in space, and the uniform pressure assumption should be valid. In fact, there are virtually no differences in the computed minimum ignition energies for an ignition time of $100 \mu s$, as can be seen in Fig. 5.

Figure 5 also shows the dependence of minimum ignition energies on the radius of the external energy source for spherical geometry in a 2:1:10 hydrogen-oxygen-nitrogen mixture at an initial pressure of 1 bar and with an ignition time of $100 \mu s$. The slope of the curve indicates that the minimum ignition energies are proportional to the source volume or, in other words, that the minimum energy density for ignition is nearly constant. In contrast to the results of Oran et al. [14] we do not find the minimum ignition energies to depend on the source radius in this range of conditions.

The dependence of minimum ignition energies on the radius of the external source for different source times is shown in Figs. 6 and 7, both for cylindrical and spherical geometry, and was calculated assuming uniform pressure. As in Fig. 5, the slope of the curve shows that if the radius is sufficiently large, the minimum energy densities necessary for ignition are nearly independent of the radius of the external source. For smaller radii, diffusion and heat conduction cause the temperature in the ignition volume to decrease and the

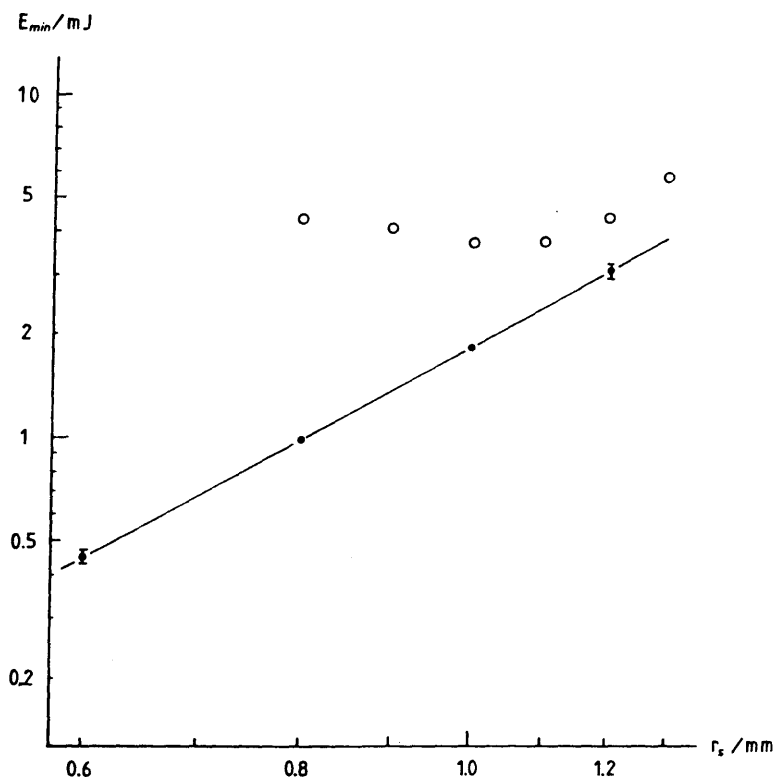


Fig. 5. Calculated minimum ignition energies in 2:1:10 hydrogen-oxygen-nitrogen mixtures for different radii of the external energy source: spherical geometry, $P = 1$ bar, $\tau_s = 0.1$ ms, 0 calculated (Oran et al. [14]): • calculated using the uniform pressure assumption (this work): ○ calculated without using the uniform pressure assumption (this work).

energy densities necessary for ignition to increase (corresponding to the curvature of the lines in Figs. 6 and 7). For short ignition times, the deviation from ideal behaviour (proportionality of minimum ignition energy and source volume) occurs at smaller radii, because the time scale of heating by the artificial energy source is shorter than the time scale of diffusion and heat conduction. These figures show that minimum ignition energies depend on the source radius, and that minimum energy densities increase with decreasing source radius (for small radii). But in fact, graphs of minimum ignition energies versus source radii are strictly monotonic, which means that the total amount of energy necessary to ignite the mixture cannot increase with decreasing source radius.

This can be easily explained if one considers two different source volumes heated by the same amount of energy. Even if diffusive and conductive processes cause energy in the smaller ignition volume to move out of this domain, the energy density is still higher than in the large source

volume. In other words, if the quenching distance is defined as the source radius where minimum ignition energy densities become substantially dependent on the source radius, then there exists a quenching distance which depends on the source time, geometry and pressure. But if the quenching distance is defined as the distance where minimum ignition energies increase with decreasing source radius, then there is no quenching distance for the problems discussed here. Such quenching distances are observed in experiments where ignition is performed by intrusive methods, for example, spark ignitions [42]. In these cases the electrodes act as a heat sink and suppress ignition of the mixture.

A comparison of the dependence of minimum ignition energies on the source radius for two different pressures (1 bar and 3 bar) is shown in Fig. 8. At higher pressures where diffusion coefficients are smaller, minimum ignition energy densities depend less on the radius of the artificial energy source.

Figure 9 shows the influence of the pressure on

Fig. 6. Ignition energy densities versus source radius for 2:1:10 hydrogen-oxygen-nitrogen mixtures at $P = 1$ bar.

minimum ignition energy densities versus source radius for 2:1:10 hydrogen-oxygen-nitrogen mixtures at $P = 1$ bar. The y-axis is logarithmic, ranging from 10^{-6} to 10^0 mJ/m³. The x-axis is linear, ranging from 0.6 to 1.2 mm.

The quenching distance is defined as the source radius where minimum ignition energy densities become substantially dependent on the source radius. Such quenching distances are observed in experiments where ignition is performed by intrusive methods, for example, spark ignitions [42]. In these cases the electrodes act as a heat sink and suppress ignition of the mixture.

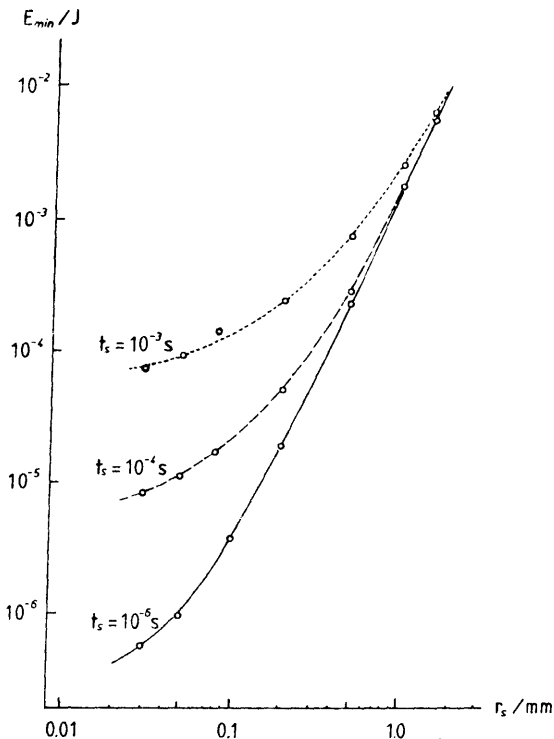


Fig. 6. Calculated minimum ignition energies in 2:1 hydrogen-oxygen mixtures for different radii of the external energy source (uniform pressure assumption: spherical geometry, $P = 1$ bar; --- $\tau_s = 1$ ms, -- $\tau_s = 0.1$ ms, — $\tau_s = 1$ μ s.

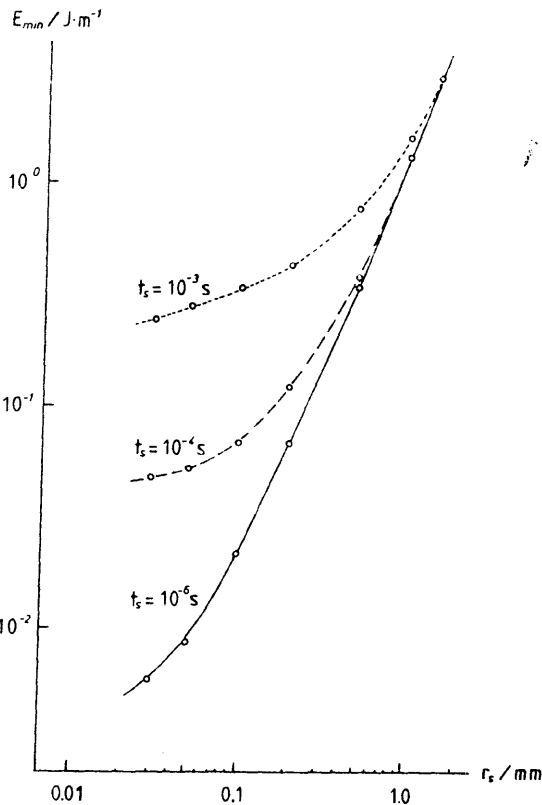


Fig. 7. Calculated minimum ignition energies in 2:1 hydrogen-oxygen mixtures for different radii of the external energy source (uniform pressure assumption): cylindrical geometry, $P = 1$ bar; --- $\tau_s = 1$ ms, -- $\tau_s = 0.1$ ms, — $\tau_s = 1$ μ s.

minimum ignition energies. Higher pressures correspond to higher heat capacities in the source volumes and, as a consequence, minimum ignition energies rise with increasing pressure. Whereas at high pressures minimum ignition energies are nearly proportional to the pressure, diffusion causes the minimum ignition densities to increase at lower pressures.

The variation of minimum ignition energies with the mixture composition is shown in Fig. 10. There is almost no dependence of the minimum ignition energies on the mixture composition for a source radius of 1 mm unless the mixture composition exceeds the flammability limits. At a mixture composition of about 4% H_2 and 96% O_2 , there is a immediate rise in minimum ignition energies. In the neighborhood of this flammability limit flame fronts are very smooth, and flames that begin to propagate occasionally die out after some time, depending on the amount of energy deposited during the ignition. For small ignition radii (calculation performed here for 0.2 mm) the minimum ignition energies become dependent on the mixture

composition because diffusion becomes important. Rich mixtures (with a large amount of rapidly diffusing hydrogen) need a higher minimum ignition energy than lean mixtures. Calculations of minimum ignition energies in the $CO-H_2-O_2$ system [39] give results similar to the H_2-O_2 system and indicate that hydrogen does not behave as an anomalous fuel with respect to these phenomena.

Pressure and Temperature Ignition Limits

Ignition limits are determined by simulating the reaction in closed vessels for various initial pressures and temperatures. This approach allows one to observe the spatial and temporal dependence of temperature and species concentrations. Other methods, such as that of Kordylewski and Scott [40], use a quasistationary state model to determine the explosion limits (assuming negligible reactant consumption and spatially uniform temperature). In fact, computations show that even

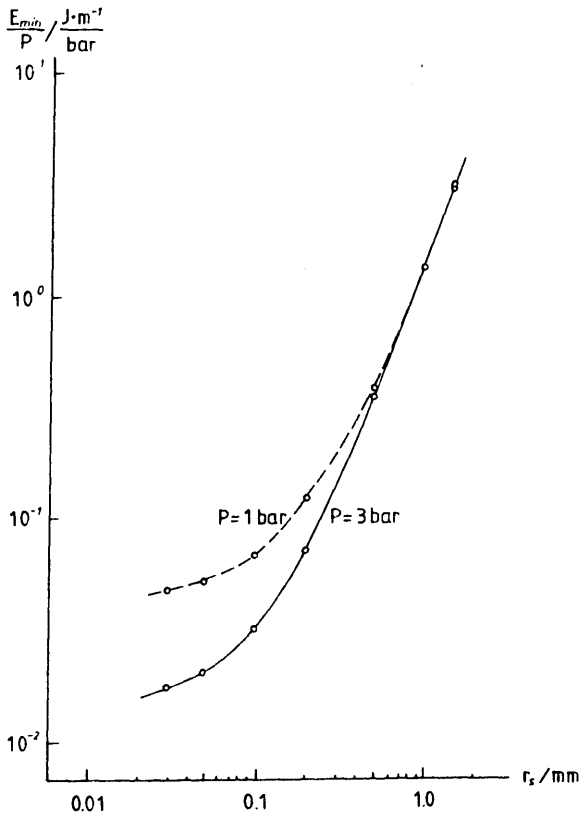


Fig. 8. Calculated minimum ignition energies in 2:1 hydrogen-oxygen mixtures for different radii of the external energy source (uniform pressure assumption): cylindrical geometry, $\tau_s = 0.1$ ms, -- $P = 1$ bar, — $P = 3$ bar.

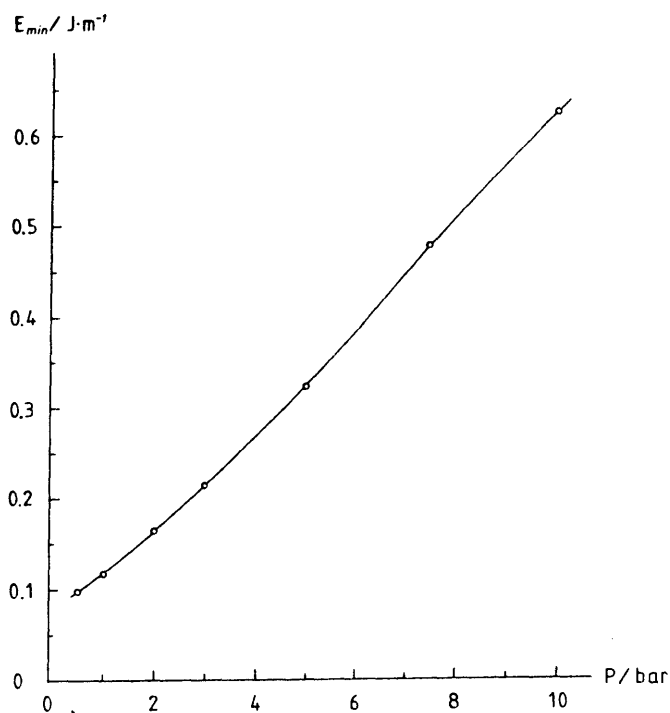


Fig. 9. Calculated minimum ignition energies in 2:1 hydrogen-oxygen mixtures for different pressures (uniform pressure assumption): cylindrical geometry, $\tau_s = 0.1$ ms, $r_s = 0.2$ mm.

during the slow reaction between the explosion limits there is a spatial dependence of the temperature, with the maximum at the vessel center. At the explosion limits, there is a quite sharp transition from slow reaction (moderate temperature rise over a long time, sometimes more than 100 s) to ignition (with an immediate temperature rise in the vessel center and propagation of the flame). Calculated pressure and temperature ignition limits for hydrogen-oxygen mixtures are shown in Fig. 11. Calculated and experimental values are in quite good agreement. Figure 11 also shows the influence of the surface destruction coefficient on the ignition limits. The small difference in the results using $\gamma = 10^{-2}$ and $\gamma = 10^{-3}$ may be explained by the fact that, for these values, the rate of the surface reactions is controlled mainly by the diffusion velocity of the species to the wall. But the increase of the second explosion limit for the small surface destruction efficiency $\gamma = 10^{-4}$ indicates that, even in boric-acid-coated vessels, surface destruction of reactive species has to be taken into account.

In accordance with the common explanation of the second explosion limit [30], sensitivity tests (Figs. 12 and 13) show that the location of the

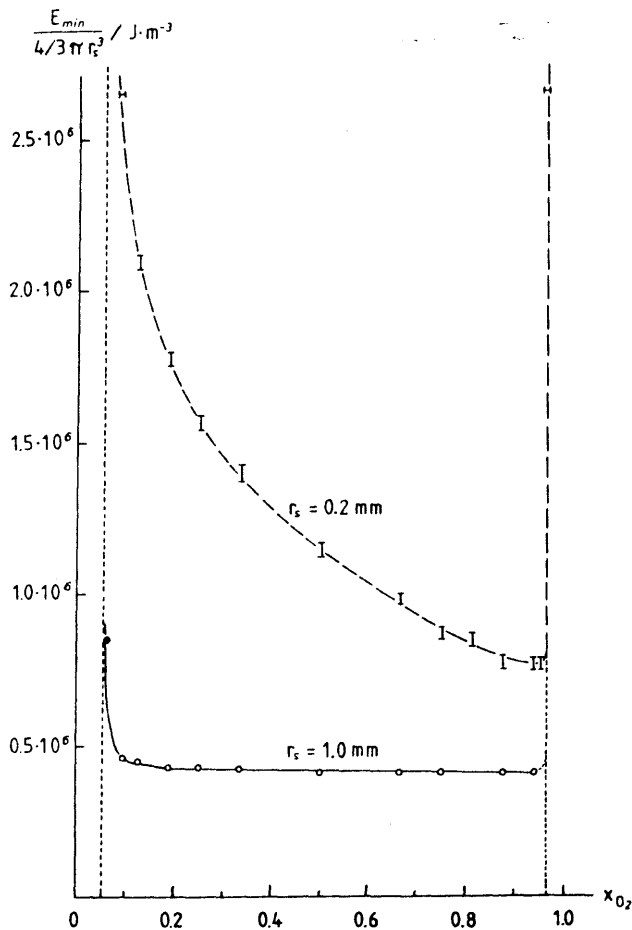


Fig. 10. Calculated minimum ignition energies in hydrogen-oxygen mixtures for different mixture compositions (uniform pressure assumption): spherical geometry, $\tau_s = 0.1$ ms, $P = 1$ bar; -- $r_s = 0.2$ mm, - $r_s = 1.0$ mm.

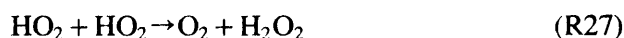
second explosion limit is controlled mainly by the rate of the chain branching reaction



and reaction R15, which produces HO_2 , a species of low reactivity,



In addition to reactions R1 and R15, the location of the third explosion limit is also sensitive to reaction R27, R29 and R32, which open up an additional pathway for the production of OH:



The rate coefficients of other reactions (including the heterogeneous reactions) have a minor influence on the second and third limit pressure. Of the surface reactions, only the destruction rate of HO_2 influences the location of the second explosion limit significantly. One question discussed very often in the literature [29, 40 and 41] is the effect of self-heating on the explosion limits. The present model, which allows for reactant consumption, shows that if a constant temperature is maintained over the entire reaction volume (the energy conservation equation is replaced by the simple condition $\partial T / \partial r = 0$), there is no longer a sharp transition from slow reaction to ignition in the region of the third explosion limit, but a steady increase of reaction rate with increasing pressure.

The surface destruction coefficient exerts a much stronger influence on the first explosion limit, which can be explained by the fact that at low pressures diffusion of the species to the wall occurs so rapidly that the surface reaction itself is rate-limiting. Limits are shown in Fig. 11 both for surface destruction coefficients, $\gamma = 10^{-3}$, for all surface reactions and for temperature dependent surface destruction coefficients [23, 25]

$$\gamma_{40} = 4.6 \cdot 10^{-2} \exp\langle -23.6 \text{ kJ}/(\text{mol R T}) \rangle$$

$$\gamma_{38} = \gamma_{39} = \gamma_{41} = \gamma_{42} = 6.3 \cdot 10^{-4}$$

$$\times \exp\langle -7.15 \text{ kJ}/(\text{mol R T}) \rangle$$

Figure 14 shows the influence of the mixture composition on the second explosion limit. The location of the explosion limit strongly depends on the third body collision efficiencies in the reaction of hydrogen atoms with molecular oxygen



Collision efficiencies derived from simple kinetic models for the second explosion limit cannot be used if detailed chemistry and species transport are used in the simulations.

Long reaction times in the slow reaction between hydrogen and oxygen allow diffusion of reactive species to the surface of the reaction

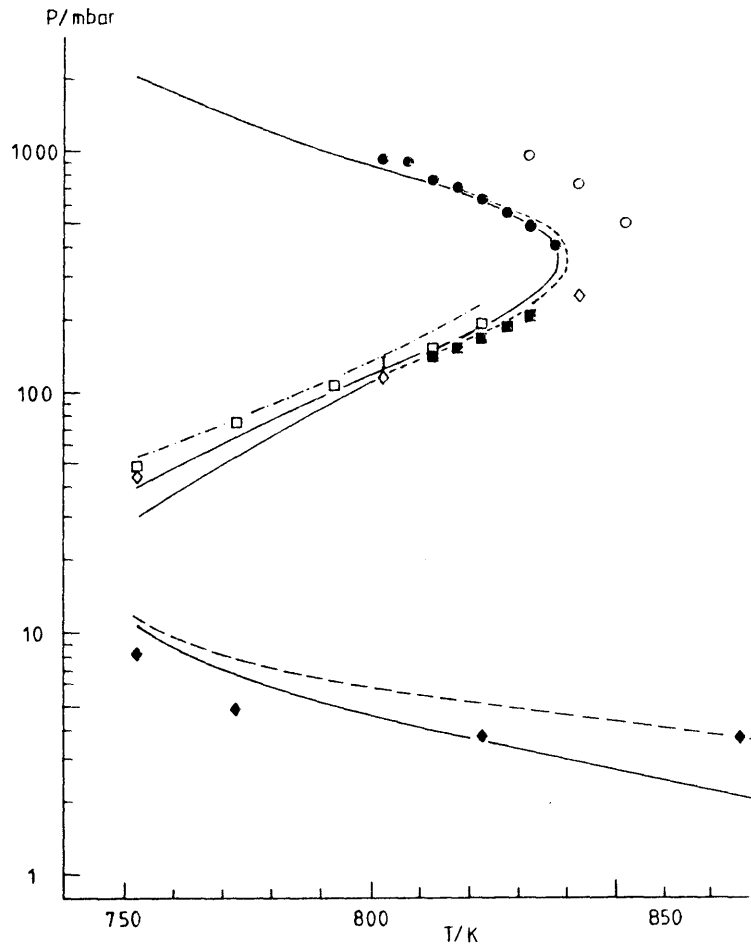


Fig. 11. Calculated and experimental ignition limits for 2:1 hydrogen-oxygen mixtures in a spherical reaction vessel 7.4 cm in diameter: -- calculated, $\gamma = 10^{-2}$; — calculated, $\gamma = 10^{-3}$; - - - calculated, $\gamma = 10^{-4}$. Experimental results: ■ thinly KCl-coated vessel [29], ○ heavily KCl-coated vessel [29], ● KCl-coated vessel [29], ◇ KCl-coated vessel [30], I clean Pyrex vessel [30], □ B_2O_3 -coated vessel [31]. Calculated and experimental first explosion limit in a cylindrical silica reaction vessel 1.8 cm diameter: ◆ experimental [32]; — calculated, $\gamma = 10^{-3}$; - - - calculated, γ see text.

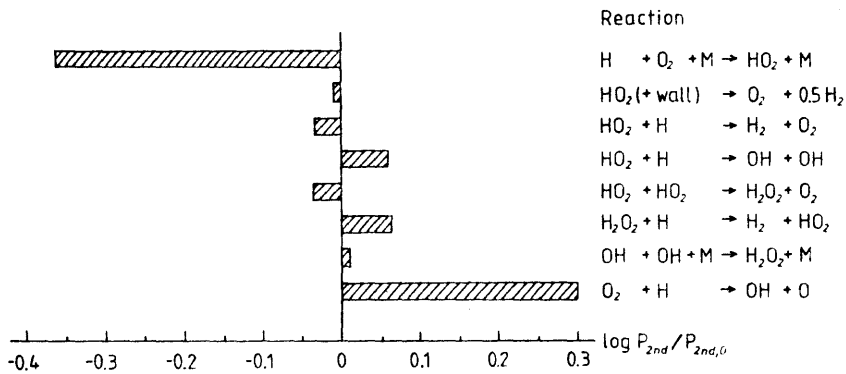


Fig. 12. Sensitivity test for the second explosion limit in a stoichiometric H_2-O_2 mixture at 803.2 K; $P_{2nd,0}$ refers to limit pressure with unchanged rate coefficients. P_{2nd} refers to limit pressure after an increase in the rate coefficient of the reaction considered and its reverse reaction by a factor of two.

vessel
exert
rate.
during
destr
ment
preci
essen
react

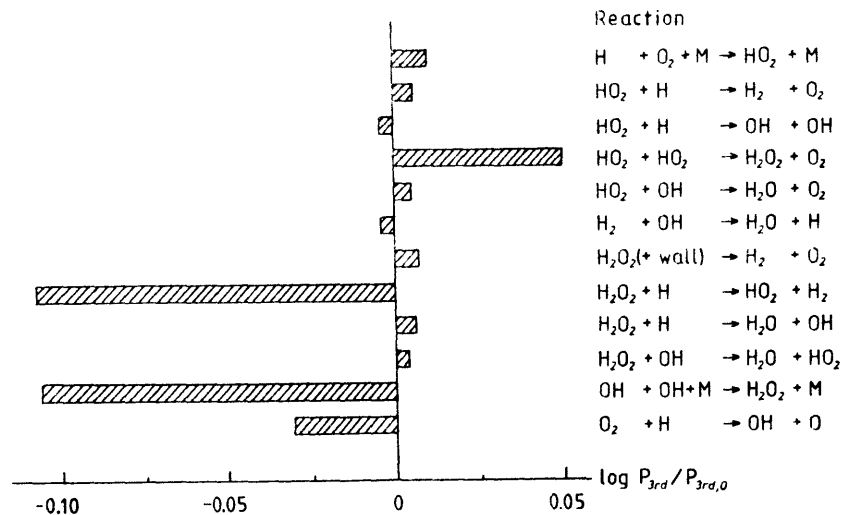


Fig. 13. Sensitivity test for the third explosion limit in a stoichiometric H₂-O₂ mixture at 803.2 K; P_{3rd,0} refers to limit pressure with unchanged rate coefficients, P_{3rd} refers to limit pressure after an increase in the rate coefficient of the considered reaction and its reverse reaction by two.

vessel. The rate of surface reactions therefore exert a strong influence on the overall reaction rate. In Fig. 15, calculated pressure changes during the slow reaction for three different surface destruction efficiencies are compared with experimental values [34]. This example shows that precise data on surface destruction efficiencies are essential for reasonable simulations of the slow reaction.

CONCLUSION

1. New numerical methods for solving stiff partial differential equations and the availability of fast computers now allow the simulation of time-dependent one-dimensional ignition processes in hydrogen-oxygen mixtures without restriction to uniform pressure distributions and using detailed chemistry and a multispecies

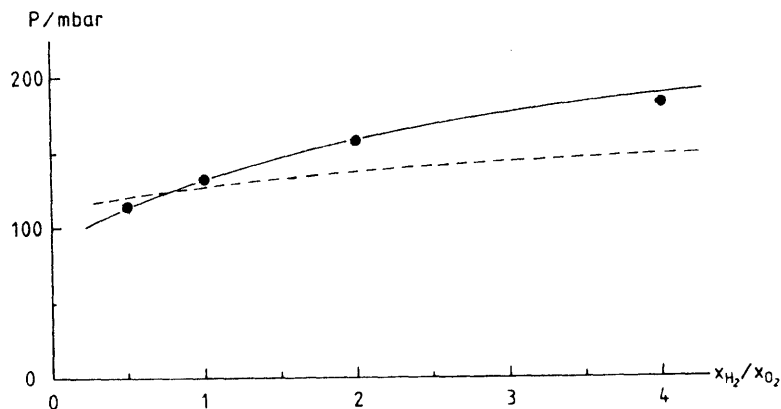


Fig. 14. Second explosion limits for mixtures of varying composition in a spherical KCl-coated vessel, 7.4 cm in diameter, T = 803.2 K; • experimental [33], -- calculated (γ = 10⁻³). Third body collision efficiencies f: f(H₂) = 1.0, f(O₂) = 0.4 and f(H₂O) = 6.5; - - calculated (γ = 10⁻³), third body collision efficiencies as above, but f(H₂) = 1.1 = f(O₂) = 0.25 and f(H₂O) = 6.5 for reaction R15.

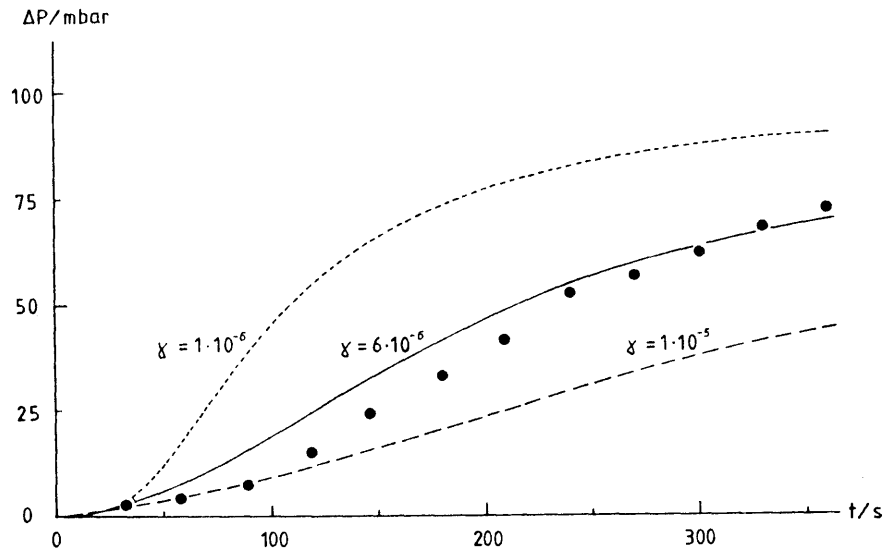


Fig. 15. Pressure change during the slow reaction of a hydrogen-oxygen mixture (28% H₂ and 72% O₂) at 773.2 K and an initial pressure of 666 mbar in a cylindrical boric-acid-coated vessel (51 mm in diameter), • experimental [34]; -- calculated ($\gamma = 10^{-5}$), — calculated ($\gamma = 6 \cdot 10^{-6}$), --- calculated ($\gamma = 10^{-6}$).

transport model. No operator splitting techniques have to be applied.

- Comparison with experimental results show that one common reaction mechanism describes shock-tube induced ignitions (simulated by treating the reaction system as a homogeneous mixture heated up by the shock wave), as well as the three explosion limits of the hydrogen-oxygen system.
- The assumption of a spatial uniform pressure is not necessary but simplifies the simulations to a great extent.
- As comparisons between calculations that incorporate the "uniform pressure assumption" and calculations that take into account spatial pressure fluctuations show, minimum ignition energies can be calculated using the uniform pressure assumption if ignition times are sufficiently long.

REFERENCES

- Baulch, D. L., Drysdale, D. D., Horne, D. G., and Lloyd, A. C., *Evaluated Kinetic Data for High Temperature Reactions*. Butterworths, London, 1972, vol. 1.
- Warnatz, J., in *Combustion Chemistry* (W. C. Gardiner Ed.), Springer, New York, 1984.
- Dixon-Lewis, G., and Williams, D. J., in *Comprehensive Chemical Kinetics*, (C. H. Bamford and C. F. H. Tipper, Eds.), Elsevier, Oxford, 1977.
- Gardiner Jr., W. C., Wakefield, C. B., Walker, B. F., in *Shock Waves in Chemistry and Chemical Technology* (A. Lifshitz, Ed.), Marcel Dekker, New York, 1981.
- Warnatz, J., *Ber. Bunsenges. Phys. Chem.* 82:643 (1978).
- Warnatz, J., *Ber. Bunsenges. Phys. Chem.* 82:834 (1978).
- Numerical Methods in Laminar Flame Propagation*, (N. Peters and J. Warnatz, Eds.), Vieweg, Braunschweig, 1982.
- Behrendt, F., and Warnatz, J., *Hydrogen Energy Progress* 5:1515 (1984).
- Behrendt, F., and Warnatz, J., *International Journal of Hydrogen Energy* 10:749 (1985).
- Warnatz, J., *Comb. Sci. Technol.* 26:203 (1981).
- Dixon-Lewis, G., Sutton, M. M., and Williams, A., *Proc. Roy. Soc.* A317:227 (1970).
- Dixon-Lewis, G., and Shepherd, I. G., *15th Symposium (International) on Combustion*. The Combustion Institute, Pittsburgh, 1975, p. 1483.
- Warnatz, J., in *Numerical Methods in Laminar Flame Propagation*. (N. Peters and J. Warnatz Eds.), Vieweg, Braunschweig, 1982, p. 87.
- Kailasanath, K., Oran, E. S., Boris, J. P., and Young, T. R., in *Numerical Methods in Laminar Flame Propagation*. (N. Peters and J. Warnatz Eds.), Vieweg, Braunschweig, 1982, p. 152.
- Wiriyawit, S., and Dabora, E. K., *20th Symposium (International) on Combustion*. The Combustion Institute, Pittsburgh, 1985, p. 179.
- Lutz, A. E., Kee, R. J., and Dwyer, H. A., *Progr. Aeronaut. Astronaut. AIAA* (1986), in press.

17. R
K
(1
18. M
S
b
19. F
C
20. P
ti
to
W
21. D
t
S
22. R
i
C
23. C
5
24. V
25. S
26. S
4
27. S
2
28. V
C
2
29. F
(

17. Raffel, B., Warnatz, J., Wolff, H., Wolfrum, J., and Kee, R. J., *Progr. Aeronaut. Astronaut.*, AIAA (1986), in press.
18. Maas, U., Raffel, B., Warnatz, J., and Wolfrum, J., 21th Symposium (International) on Combustion. The Combustion Institute, Pittsburgh, 1987, in press.
19. Fritsch, F. N., and Butland, J., *SIAM J. Sci. Stat. Comput.* 5:300 (1984).
20. Petzold, L. R., *A Description of DASSL: A Differential/Algebraic System Solver*. Sandia National Laboratories, Report SAND 82-8637, Livermore, 1982; IMACS World Congress, Montreal, 1982.
21. Deuffhard, P., and Nowak, U., *Extrapolation Integrators for Quasilinear Implicit ODEs*. Univ. Heidelberg, SFB 123: Tech. Rep. 332, 1985.
22. Richtmyer, R., and Morton, K., in *Interscience Tracts in Pure and Applied Mathematics No. 4*, (L. Bers, R. Courant, and J. Stoker, Eds.), second edition.
23. Greaves, J. C., and Linnet, J. W., *Trans. Faraday Soc.* 54:1323 (1958); 55:1338 (1959).
24. Wise, B. J., *J. Phys. Chem.* 66:1049 (1962).
25. Smith, W. V., *J. Chem. Phys.* 11:110 (1943).
26. Skinner, G. B., and Ringrose, G. H., *J. Chem. Phys.* 42:2190 (1965).
27. Schott, G. L., and Kinsey, J. L., *J. Chem. Phys.* 29:1177 (1958).
28. Voevodsky, V. V., *R. I. Soloukhin 10th Symp. (Intl.) Comb.*, The Combustion Institute, Pittsburgh, 1964, p. 279.
29. Heiple, H. R., and Lewis, B., *J. Chem. Phys.* 9:584 (1941).
30. von Elbe, G., and Lewis B., *J. Chem. Phys.* 10:366 (1942).
31. Egerton, A. C., and Warren D. R., *Proc. Roy. Soc. A204:465 (1951)*.
32. Hinshelwood, C. N., and Moelwyn-Hughes, E. A., *Proc. Roy. Soc. London A138:311 (1932)*.
33. Baldwin, R. R., *Trans. Faraday Soc.* 52:1344 (1956).
34. Baldwin, R. R., and Mayor, L., *Trans. Faraday Soc.* 56:80 (1960).
35. Warnatz, J., in *Combustion Chemistry* (W. C. Gardiner Jr., Ed.), Springer, New York, 1984.
36. Frenklach, M., and Warnatz, J., *Comb. Sci. Technol.* 51:265 (1987).
37. Warnatz, J., publication in preparation.
38. Behrendt, F., and Warnatz, J., *Int. J. Hydrogen Energy* 10:749 (1985).
39. Maas, U., and Warnatz, J., 22nd Symposium (International) on Combustion (1988), accepted for presentation.
40. Kordylewski, W., and Scott, S. K., *Comb. Flame* 57:127-139 (1984).
41. Griffiths, J. F., Scott, S. K., and Vandamme, R., *J. Chem. Soc., Faraday Trans. I*, 77:2265-2270 (1981).
42. Lewis, B., and von Elbe, G., *Combustion, Flames and Explosions of Gases*, Academic Press, New York, 1961.

Received 10 July 1987; revised 7 January 1988

C. F. H.
B. F., in
chnology
, 1981.
82:643
82:834

agation,
Braunsch-

Energy

ournal of

81).
ams, A.,

mposium
ion Insti-

ar Flame
Vieweg,

oung, T.
e Propa-
Vieweg,

mposium
ion Insti-

, Progr.